Research Square

Preprints are preliminary reports that have not undergone peer review.
They should not be considered conclusive, used to inform clinical practice,
or referenced by the media as validated information.

Molecular Dynamics Investigation of Solid Methane Crystal Storage in Coal Matrix Confined Pores: A Potential Trigger Mechanism for Coal Outbursts

Wei Chen

timtamu@suda.edu.cn

Soochow University

Junjie Niu

Soochow University

Yilin Chen

China University of Mining and Technology

Research Article

Keywords: Methane, Interfacial growth, Outburst, Face-centered cubic, Crystallization

Posted Date: November 18th, 2026

DOI: https://doi.org/10.21203/rs.3.rs-11453359/v1

License: This work is licensed under a Creative Commons Attribution 4.0 International License.
Read Full License

Additional Declarations: No competing interests reported.

Molecular Dynamics Investigation of Solid Methane Crystal Storage in Coal Matrix Confined Pores: A Potential Trigger Mechanism for Coal Outbursts

Wei Chen*[a], Junjie Niu [a], Yilin Chen*[b]

[a] School of Rail Transportation, Soochow University, Suzhou 215131, China
[b] Key Laboratory of Coalbed Methane Resources and Reservoir Formation Process of the Ministry of Education, China University of Mining and Technology, Xuzhou, 221008, China

*Corresponding Author： Wei Chen， Yilin Chen

Email: timtamu@suda.edu.cn

Abstract

Coalbed methane (CBM) outbursts pose critical safety risks, with incompletely clarified mechanisms for anomalous gas storage. This study proposes that interfacial growth-driven solid methane storage in coal matrices arises from lattice-matched crystallization at NaCl-CH_4 interfaces—enabled by the near-identical face-centered cubic (FCC) lattice constants of NaCl (5.640 Å) and CH_4 (5.665 Å)—which potentially trigger outbursts. To verify this, molecular dynamics (MD) simulations probed methane crystallization in FCC-NaCl nanopores under four pressures (S1–S4: 50, 97, 145, 176 MPa) during 400 K→30 K thermal quenching. Results reveal a hierarchical crystallization pathway: methane first forms dense wall monolayers, followed by bulk FCC lattice nucleation at ~140 K (confirmed by radial distribution function, RDF), driven by interfacial lattice compatibility that induces symmetry-aligned molecular ordering; pressure governed phase distribution, with lower pressures (e.g., S1) favoring surface adsorption and higher pressures (e.g., S4) promoting bulk crystallization (evidenced by plateaued mean-squared displacement, MSD, indicating long-range crystalline order). Between 140–92 K, structural entropy and diffusion coefficients dropped sharply as methane stabilized into ordered FCC configurations within NaCl-structured nanopores, and notably, metastable methane accumulation at ~140 K caused localized near-vacuum conditions that stabilized clathrate-like structures, enabling coal methane storage capacities far exceeding Langmuir adsorption model predictions by orders of magnitude.

Key Words: Methane, Interfacial growth, Outburst, Face-centered cubic, Crystallization

Introduction

Gas outbursts in underground coal mining present severe safety hazards through sudden, violent releases of gas (CH_4, CO_2, or both) and pulverized coal debris from seams or rock formations, endangering workers and infrastructure[1, 2]. These explosive, short-lived events are intricately linked to tectonic coal—structurally deformed by tectonic forces—which exhibits compromised microstructural integrity (e.g., fractured matrices, porous networks), heightening its propensity for outbursts[3-5]. The interplay of gas pressure and coal fragmentation during these phenomena underscores their destructive complexity[6].

Notably, coalbed outbursts release methane volumes far exceeding theoretical adsorbed gas capacities, with documented gas-to-coal ratios surpassing 132 m^3/t (e.g., Daping Mine) [7-9]. These events are hypothesized to originate from tectonic stress-induced structural reorganization in coal, which elevates aromatic hydrocarbon content and enhances methane adsorption affinity—despite reduced porosity—thereby amplifying gas retention in deformed coal matrices [10-12]. During outbursts, high-pressure gas accumulations near fracture networks violently eject thousands of tons of pulverized coal through confined pathways at extreme velocities, sustained by rapid gas expansion during decompression [8, 13]. However, the mechanisms enabling long-term retention of high-pressure gas in damaged coal structures—and their direct role in transitioning from gradual gas accumulation to catastrophic outburst initiation—remain unresolved, with a critical knowledge gap in both predicting and mitigating these disasters.

Significant efforts have employed mechanistic modeling to address these challenges. For instance, Hao et al. integrated gas desorption-seepage equations with stress analyses through multi-physics coupling [14], while Yan et al. demonstrated that geo-storage anomalies—quantified via seismic velocity inversions—serve as robust precursors for outburst-prone zones in deep Chinese mines [15]. Despite 160 years of empirical and theoretical investigation, the multiscale physics governing coal-gas outbursts remain elusive, particularly the phase behavior of high-pressure methane under tectonic confinement and its nonlinear coupling with fracture propagation [16]. The mechanistic basis of coal's anomalous gas storage capacity—central to outburst dynamics—remains unresolved, impeding hazard mitigation even as understanding of initiation processes advances [17, 18]. Critical gaps persist in explaining outburst gas volumes that exceed model-predicted adsorbed/free gas maxima by three orders of magnitude, a discrepancy most pronounced in tectonically altered, organic-rich

coals[19].

Recent advances in gas storage mechanisms reveal that coal and shale nanopores exhibit anomalous methane retention exceeding predictions from classical adsorption models, driven by confinement-induced non-ideal gas interactions. Chen et al. demonstrated supercritical methane densification in nanoconfined pore systems (<10 nm diameter), where pore wall interactions and spatial constraints amplify gas density beyond conventional thermodynamic expectations [19], Similarly, Wang et al. established a dual-site Langmuir model to account for supercritical methane adsorption in deep coal seams (>1000 m depth), resolving discrepancies in high-pressure adsorption isotherms through heterogeneous surface energy distributions) [20]. Experimental studies further identify metastable methane hydrates (e.g., Type I/II clathrates) forming at pressures exceeding 10 MPa within tectonically damaged, low-permeability coal matrices, where hydrophilic mineral interfaces act as nucleation templates by stabilizing hydrate cages through hydrogen bonding [21-23]. However, direct evidence of *in-situ* methane hydrates in fractured or structurally damaged coal systems remains elusive, with hypothesized tectonic stress-modulated hydrate-gas phase coexistence lacking field validation via advanced geophysical imaging or pressure-preserved core sampling [25].

Interface-controlled crystal growth mechanisms, leveraging face-centered cubic (FCC) or hexagonal close-packed (HCP) frameworks, have been widely studied in advanced materials (e.g., high-strength alloys, glass ceramics) for their ability to stabilize interfacial architectures under extreme thermodynamic conditions [20-22]. Within coal matrices, sodium chloride (NaCl)—a naturally occurring inorganic compound exhibiting FCC lattice symmetry with lattice constants 5.640 Å, serves dual roles as a catalytic template for interfacial reactions and a combustion byproduct [23, 24]. Recent advancements suggest that nanoscale mineral interfaces, notably FCC-aligned NaCl crystallites, can template methane solidification into stabilized clathrates within coal nanopores through epitaxial alignment, representing a transformative gas storage mechanism. These mechanisms, governed by lattice-matching interactions similar to those observed in metal/ceramic composites [25-27], achieves methane densification significantly exceeding classical sorption models. However, the hypothesized mechanism of methane crystallization within NaCl-coated nanopores remains

unproven, lacking empirical validation or computational simulations.

This study employs molecular dynamics (MD) simulations to investigate methane solidification within NaCl-constructed nanopores across four distinct systems, analyzing nucleation dynamics during controlled crystallization processes. Thermodynamic and kinetic parameters—including system pressure and entropy fluctuations—were quantified to map metastable states and identify phase transition thresholds, while radial distribution function (RDF) analysis revealed structural evolution through crystallographic signatures of methane's short- and long-range ordering. Further, mean squared displacement (MSD) and diffusivity variations were evaluated to disentangle molecular mobility trends, elucidating how reduced kinetic freedom at critical densities drives structural transitions and stabilizes methane's solid-phase configurations.

2. Simulation Details and Methods

2.1 Modeling

The crystalline structure of sodium chloride (NaCl) in geological formations such as coal seams adopts a FCC configuration characterized by a lattice parameter of 5.64 Å (Figure 1) [28]. Significantly, structural compatibility between NaCl and solidified methane arises from their shared FCC lattice symmetry and comparable molecular dimensions (a = 5.665 Å for CH_4)[29], implying a potential mechanistic basis for methane lattice organization within coalbed matrices[30].

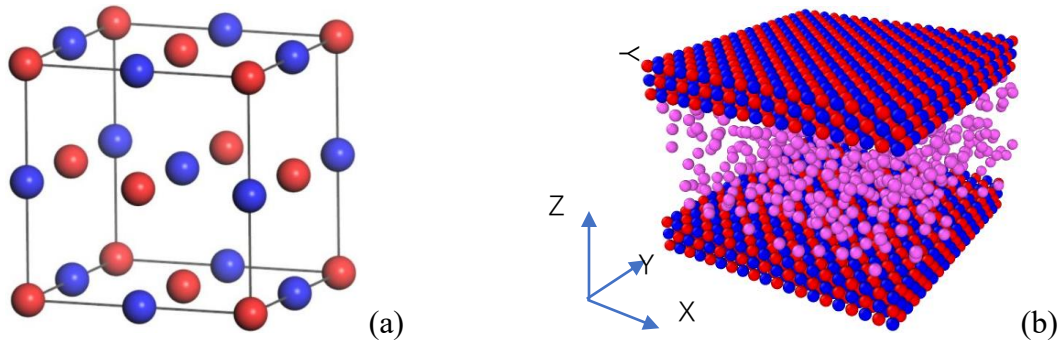


Figure 1. (a) Schematic diagram of FCC structure of NaCl crystal (Red: Na, Blue: Cl); (b) Initial configuration of NaCl crystal layers filled with CH_4 molecules in S2 system (Red: Na, Blue: Cl, Purple:CH_4).

To investigate this phenomenon, a computational model was constructed,

incorporating two parallel NaCl crystalline substrates separated along the z-axis. This configuration establishes a controlled interfacial environment to systematically study methane solidification dynamics under conditions replicating geological coalbed settings. The molecular dynamics simulations employed periodic boundary conditions (PBC) within a cuboidal simulation cell configured with dimensions of 56.4 Å × 56.4 Å × 45.12 Å, aligned orthogonally along the *x*, *y*, and *z* Cartesian axes. Interatomic interactions were modeled using the Lennard-Jones potential coupled with Coulombic interactions, with a cutoff distance set at 12 Å for both energy components:

$$u_{LJ}(r_{ij}) = 4\varepsilon_{ij}\left[\left(\frac{\sigma_{ij}}{r_{ij}}\right)^{12} - \left(\frac{\sigma_{ij}}{r_{ij}}\right)^{6}\right] \quad (1)$$

Where r_{ij} represents the separation distance between the sites *i* and *j* molecules, ε_{ij} and σ_{ij} are the depth of potential well and zero-crossing distance for the potential, respectively. The parameters of LJ potential for NaCl and CH_4 are given in Table 1 as follows:

Table 1. Lenard-Jones parameters for NaCl and CH_4.

Particles	σ (Å)	ε (Kcal/mol)	Ref.
Na^+	2.35	0.130	[31]
Cl^+	4.40	0.100	[32]
CH_4	3.73	0.293	[33]

The potential parameters between different ions follow the Lorentz-Berthelot mixing rules[34]:

$$\sigma_{ij} = \frac{\sigma_{ii}+\sigma_{jj}}{2} \quad (2)$$

$$\varepsilon_{ij} = \sqrt{\varepsilon_{ii}\varepsilon_{jj}} \quad (3)$$

For the Na^+-Cl^- interaction, the Lennard-Jones parameters—σ (collision diameter) and ε (energy well depth)—were calculated via the prescribed equation, resulting in values of 3.375 Å and 0.114 kcal/mol, respectively.

Afterwards, grand Canonical Monte Carlo (GCMC) simulations were conducted to model four discrete methane populations (549, 752, 862, and 960 molecules) within the NaCl channel under corresponding pressure conditions (70 MPa, 140 MPa, 560

MPa, and 1400 MPa, respectively). Methane was represented as monoatomic entities using unified Lennard-Jones potential spheres to enhance structural clarity and computational tractability. After the methane molecules filling was completed in the NaCl channel, energy minimization was performed via the conjugate gradient algorithm, eliminating steric clashes and stabilizing atomic configurations to a convergence criterion of 0.001 kcal/(mol·Å), thereby ensuring physically realistic initial geometries. Following equilibration, thermodynamic equilibrium pressures were quantified and compiled (Table 2), offering empirical insights into methane confinement behavior as a function of molecular density and pressure gradients within the NaCl matrix.

Table 2. Specific input parameters of four different systems

System No.	Number of CH_4 molecules	Pressure after equilibrium (MPa)
S1	549	50.0
S2	752	97.0
S3	862	145.0
S4	960	176.0

Under natural geological temperature and pressure conditions, the formation of methane crystalline domains occurs over extended geological timescales. This process presents a significant computational challenge due to the prohibitive resource demands of molecular dynamics (MD) simulations aimed at modeling such nucleation kinetics. To circumvent these spatiotemporal and resource limitations, a controlled cooling protocol was employed to artificially accelerate phase-transition dynamics. While low temperatures reduce molecular mobility, they simultaneously enhance adsorption of methane molecules onto pore surfaces, creating localized conditions that kinetically favor crystallization[35]. This approach enabled the interrogation of methane solidification pathways within computationally tractable simulation timeframes while maintaining mechanistic faithfulness to natural crystallization processes. The system was first thermally equilibrated at 400 K for 10 ps under the *NVT* ensemble using a Nosé-Hoover thermostat (relaxation time: 100 fs) to stabilize atomic configurations and minimize energy fluctuations. Methane solidification was induced by linearly cooling the system from 400 K to 30 K over 294 ps (cooling rate: 1.26 K/ps) under *NVT* conditions, followed by a 50 ps isothermal

simulation at 30 K to attain structural equilibrium. Interatomic interactions were governed by a Lennard-Jones potential with a 12 Å cutoff, and simulations were executed via the LAMMPS package across four methane population regimes (Table 2). Kinetic data and trajectory snapshots were rigorously analyzed to quantify nucleation dynamics, lattice ordering, and energy convergence, providing mechanistic insights into pressure-dependent crystallization pathways.

2.2 Radial Distribution Function (RDF) of the Methane Molecules

The radial distribution function (RDF) was employed to characterize the spatial distribution of methane molecules within NaCl nanopores post-solidification, serving as a structural probe to assess crystallinity and determine whether CH_4 molecules crystallize into ordered solid phases. The RDF, a pairwise correlation function, quantifies the probability of locating atom *j* at a radial distance *r* from a reference atom *i*, mathematically defined as[36]:

$$g(r) = \frac{n_j V}{N_j 4\pi r^2 dr} \tag{4}$$

where n_j is the number of j particles between r and r + dr from the atom i, V is the volume of the system, N_j is the total number of j particles, and $r(t_0)$ and $r(t+t_0)$ denote initial and time-evolved molecular coordinates.

2.3 Mean Square Displacement (MSD) and Diffusion coefficient of the Methane Molecules during Crystallization

During cooling-induced crystallization, methane undergoes a phase transition from a disordered fluid phase to an ordered crystalline state, mediated by CH_4-nanopore wall interactions and intermolecular cohesive forces. To quantitatively characterize the dynamic evolution of confined methane, mean square displacement (MSD) analysis was employed as a probe for diffusion kinetics, phase transformation pathways, and emergent lattice ordering[37]. The MSD, defined as the ensemble-averaged squared displacement of particles over time, is expressed mathematically as:

$$MSD = \left\langle \frac{1}{N} \sum_{i=1}^{N} \left[r_i(t + t_0) - r_i(t_0) \right]^2 \right\rangle \tag{5}$$

where $r_i(t)$ is the position of the i-th methane molecule at time t, N is the total number of molecules, and $\langle \cdot \rangle t_0$ denotes an average over initial time origins. In addition, the diffusion coefficient (D), which quantifies the proportionality between molecular mobility and temporal displacement via the Einstein relation[37]:

$$D = \lim_{t\to\infty} \frac{1}{6t} \langle [r(t+t_0) - r(t_0)]^2 \rangle \quad (6)$$

2.4 The Structure Entropy of the Crystallization System

The solidification of methane within nanopores constitutes a fundamental physical phenomenon characterized by the spontaneous self-organization of disordered gaseous-phase molecules into highly ordered FCC crystalline lattices at pore interfaces. This process elucidates phase transition mechanisms under nanoconfinement and provides a complementary framework to conventional structure prediction methods, which are predominantly grounded in energy minimization principles to identify thermodynamically stable crystalline configurations[38]. Structural entropy (*Ss*), a key thermodynamic parameter quantifying local order during solidification, was derived from the radial distribution function $g(r)$ and expressed as [39]:

$$S_s = -2\pi\rho k_B \int_0^{r_m} [g(r)lng(r) - g(r) + 1] r^2 dr \quad (7)$$

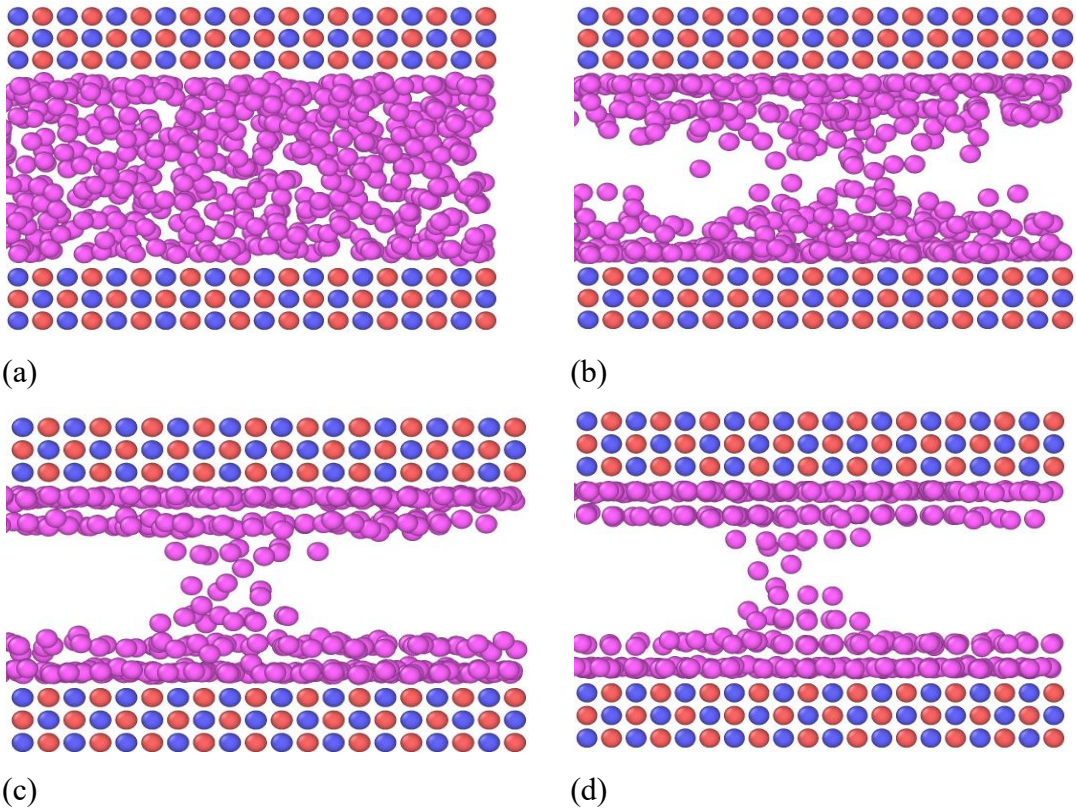
where g(r) is the radial distribution function and ρ is the density of the system. Thus, S_s could be served as a critical methodology for elucidating kinetic trajectories of solidification, developing predictive frameworks for phase transformation dynamics under nanoconfinement, and eliminating a priori assumptions regarding terminal structural configurations.

3. Results and Discussions

3.1 The Methane Molecules Crystallization in the NaCl Channels

Controlled cooling simulations facilitated methane crystallization within confined NaCl nanochannels. The molecular states of methane at 400 K, 140 K, 92 K, and 30 K were depicted in Figures 2 and 3 for systems S1 and S4, respectively. These figures illustrated the progressive organization of methane molecules within FCC-structured NaCl frameworks during crystallization. A progressive transition from stochastic molecular distributions to equilibrium architectures dominated by phase-segregated domains was observed, underscoring that interface-induced crystallization governs the emergence of ordered molecular organization within the confined NaCl matrix.

Notably, both systems exhibited increasing molecular order as temperatures decreased. A hierarchical crystallization mechanism emerged in the confined systems: methane molecules initially adsorbed onto pore surfaces as dense monolayers, followed by nucleation and growth of bulk crystalline phases. At lower pressures (e.g., S1), most molecules remained surface-adsorbed, whereas elevated pressures (e.g., S4) promoted bulk crystal formation, highlighting pressure-dependent regulation of crystallization pathways. This dual-phase behavior arises from NaCl's structural templating effect, wherein methane molecules preferentially diffuse toward NaCl crystals within the nanopores. The templating is enabled by the near-identical lattice parameters of FCC-CH_4 (5.665 Å) and NaCl (5.640 Å), which stabilize epitaxial alignment at the interface via minimal lattice mismatch (<0.5%). The geometric compatibility allows NaCl pore walls to act as nucleation sites, significantly reducing the activation energy barrier for methane incorporation into FCC lattices. By aligning methane molecules into symmetry-matched positions, the templating mechanism bypasses kinetic bottlenecks inherent to bulk-phase nucleation, thereby promoting ordered lattice assembly[40].



(a) (b)

(c) (d)

Figure 2. (a) initial state of methane molecules in S1 at 400 K;2) the state of methane molecules in S1 at 140 K;(3) the state of methane molecules in S1 at 92 K; (4) the state of methane molecules in S1 at 30K.

In contrast to other systems, spatial partitioning advanced significantly in system S4, with the majority of methane solidifying into coherent FCC lattices within central pore regions. This spatial ordering is evidenced by the radial distribution function (RDF) profiles of the molecules (see subsequent analysis). The enhanced crystallization efficiency arises from the elevated molecular density in high-pressure systems, which amplifies templating effects at NaCl-methane interfaces. This increased density promotes epitaxial lattice alignment by supplying a greater population of methane molecules for diffusion into FCC-structured domains. Consequently, gas outbursts preferentially occur in high-pressure coal matrices, where accumulated strain energy and exothermic phase transitions of methane—driven by rapid crystallization—overcome the mechanical stability of the coal lattice.

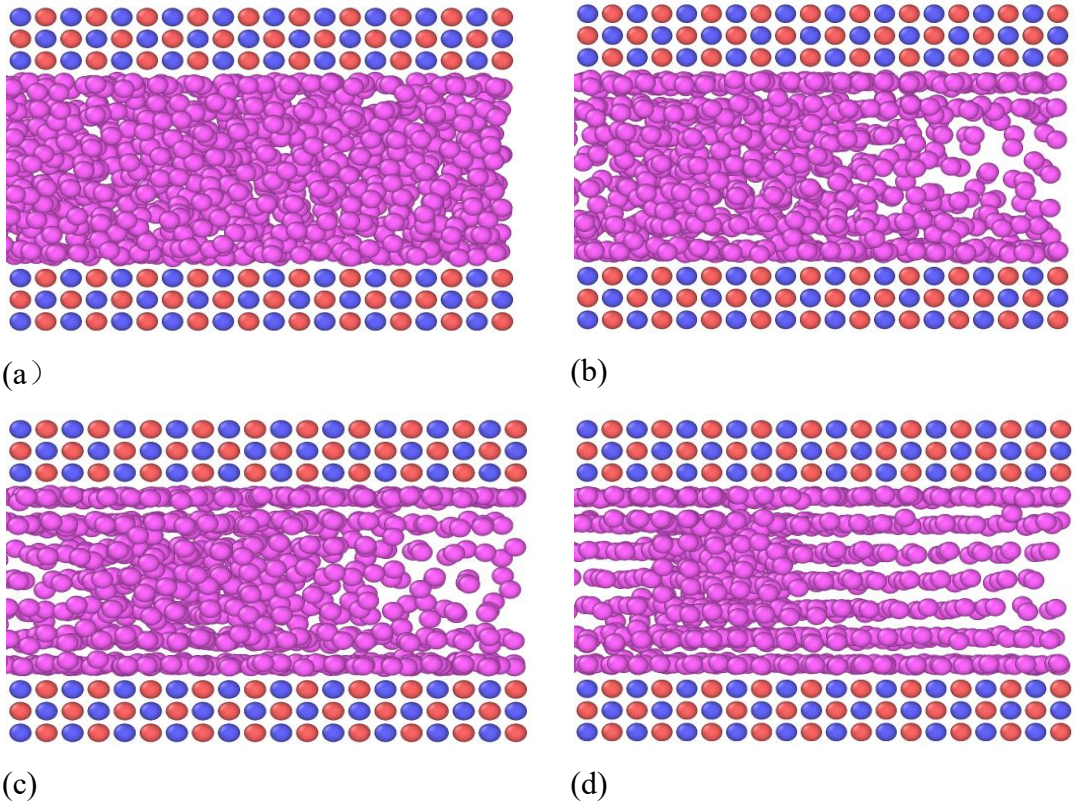


Figure 3. (a) initial state of methane molecules in S4 at 400 K;(b) the state of methane molecules in S4 at 140 K; (c) the state of methane molecules in S4 at 92 K ;(d) the state of methane molecules in S4 at 30K.

3.2 Radial Distribution Function of the Methane Molecules during Crystallization Process

Figure 4 illustrates the temporal evolution of methane molecular ordering within NaCl-structured nanopores during controlled cooling, captured at sequential temperature intervals (400 K, 270 K, 140 K, 92 K, and 30 K). Based on Eq(4), radial distribution function (RDF) analysis revealed three distinct structural signatures at 4.2 Å (nearest-neighbor spacing), 5.8 Å (unit-cell edge), and 7.2 Å (diagonal spacing), with peak intensities escalating progressively during crystallization. The dominant peak at 4.2 Å corresponds to face-diagonal molecular spacing (√2/2 lattice parameter), consistent with FCC nearest-neighbor coordination, confirming methane's transition into FCC crystalline order. Subsequent peaks at 5.8 Å and 7.2 Å align with unit-cell-edge distances and higher-order FCC packing symmetries, respectively, further corroborating crystallographic ordering. Notably, these structural signatures emerge prominently near 140 K in high-pressure systems (e.g., S3 and S4), whereas low-pressure systems (e.g., S1) already formed surface-adsorbed layers at higher temperatures due to their lower molecular density. The crystallization onset temperature of 140 K observed under nanoconfined conditions starkly contrasts with methane's standard freezing point (90.7 K at 1 atm) in macroscopic bulk systems, suggesting that surface-induced crystal growth at the CH_4-NaCl interface suppresses thermodynamic nucleation barriers—likely due to epitaxial templating and confinement effects that stabilize critical nuclei. This mechanism bypasses classical nucleation pathways by leveraging interfacial templating effects. As temperatures decrease from 140 K to 92 K, peak intensities (e.g., the 4.2 Å signature) rise sharply, particularly in high-pressure systems S3 and S4. This progression mechanistically parallels methane's phase transition from a disordered gaseous state to bulk FCC crystallization, driven by templating effects at the NaCl-methane interface [41]. Optimized ion-dipole interactions at these interfaces guide molecular alignment into symmetry-matched positions, effectively lowering the activation energy for epitaxial lattice assembly. As the temperature decreased below 92 K, the intensities of structural signatures exhibited a moderate rise across all systems. During this phase, methane molecules gradually migrated toward their lowest-energy lattice sites, ultimately forming a structurally stable, long-range-ordered crystalline framework

with a FCC arrangement[42].

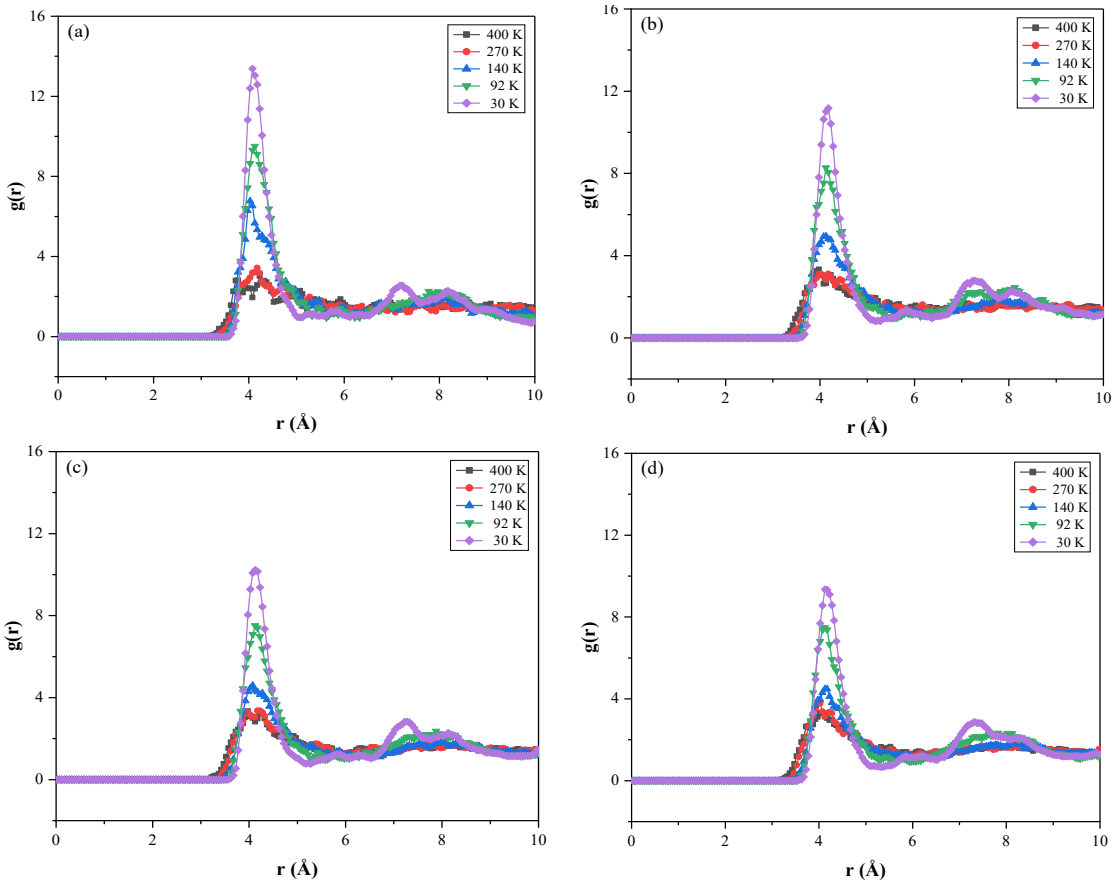


Figure 4. Radial Distribution Function of the Methane Molecules during crystallization process at 400K, 270K, 140K, 92K, and 30K (a) system S1 (b) System S2 (c) system S3 (d) system S4

3.3 System Pressure during the Crystallization Process

As the systems were subject to cooling, the pressures of the four system all decreased. Concurrent with methane crystallization, equilibrium pressures already approached 0 MPa (Figure 5) as temperatures reached above 150 K, signifying that almost all methane molecules had transitioned into a more stable crystalline structure. Upon further cooling, the FCC phase became increasingly thermodynamically stable, and a volumetric contraction emerged, generating negative pressure. The pressure decrease induced by methane crystallization reflects the absorption of substantial methane quantities from surrounding matrices into localized density anomalies ("black holes"), where molecular accumulation ratios surpassed 10^2–10^3. This arises from the extreme density contrast between solid methane (~0.5 g/cm³) and its gaseous phase (~0.0007 g/cm³) [43]. This demonstrates that geomechanical destabilization of the coal matrix

triggers crystalline lattice failure, resulting in sudden gas outbursts through exothermic solid methane phase transitions.

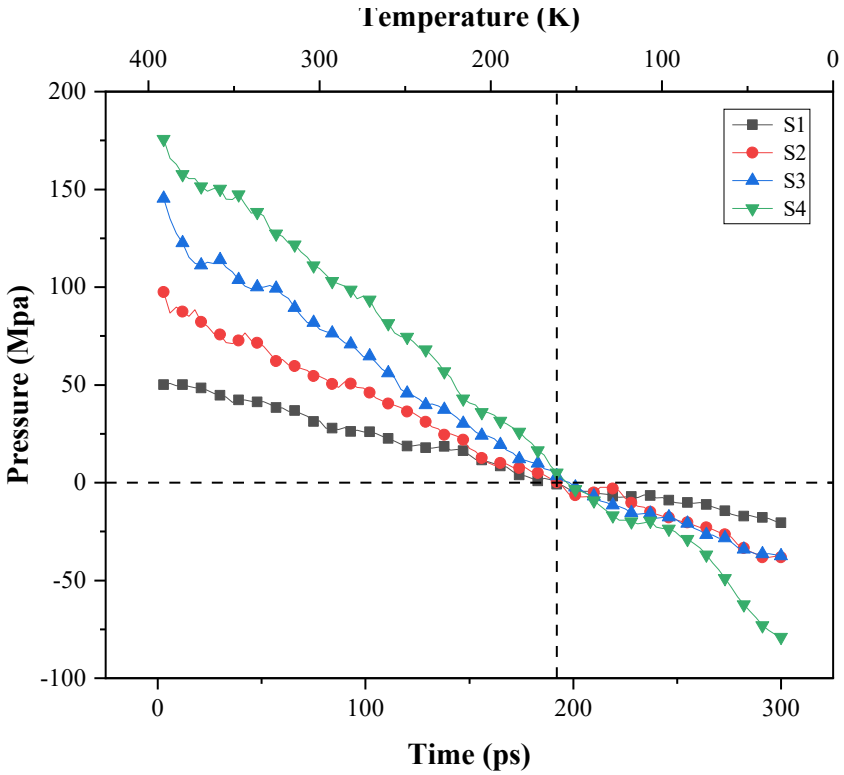


Figure 5. Temporal evolution of system pressure during methane crystallization dynamics for the four system

3.4 The Structure Entropy (S_s) of Methane Molecules during Crystallization Process

When methane was confined within NaCl-structured nanopores, its phase transition from a disordered gaseous state to an ordered FCC crystalline solid was driven by a sharp reduction in structural entropy, collapsing from -10 k_B to −18 k_B when temperature decreased from the threshold 140 K to 90 K (eg., S4) as given in Figure 6(a). This entropy-driven ordering arises from geometric templating effects imposed by the NaCl lattice, which align methane molecules with the host's cubic symmetry, overriding thermal disorder and stabilizing periodic molecular arrangements [44]. The rate of structural entropy reduction ($-dS/dt$) initiates at 200 K, accelerates markedly near 140 K (Figure 6(b)), and culminates in a sharp maximum at 92 K, signifying a rapid transition to an ordered state within this temperature regime.

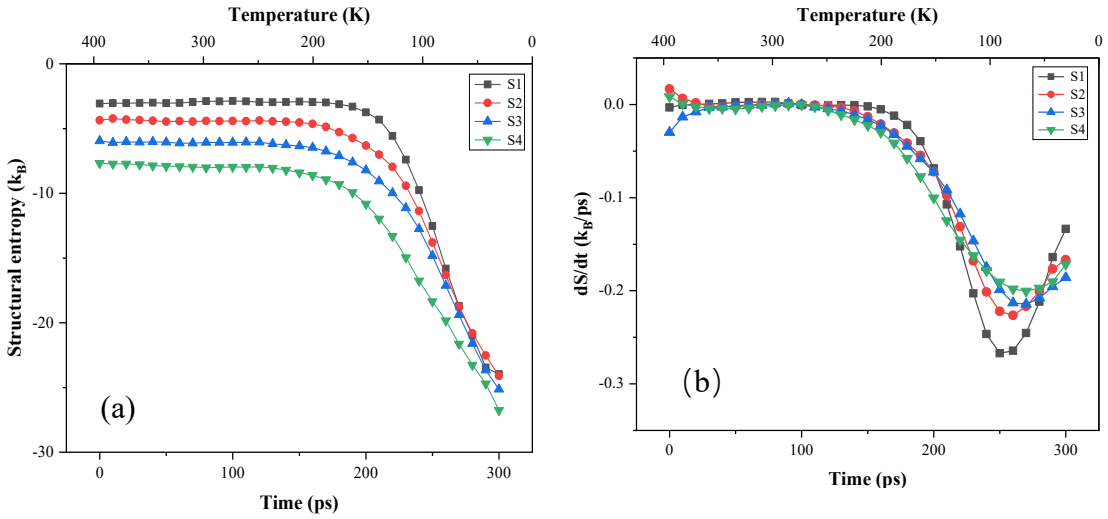


Figure 6. (a) Structure entropy of the molecules during solidification process (b) the change rate of entropy of the four systems

3.5 Mean Square Displacement (MSD) of Methane Molecules

The mean square displacement (MSD) of methane molecules within NaCl nanopores during cooling-induced solidification delineates two distinct dynamical regimes (Figure 7(a)). During the initial cooling phase (400 K → 140 K), the MSD exhibits a monotonic increase across all systems (S1–S4), with system S1 displaying the most pronounced rise, attributed to its lower molecular packing density and extended mean free path. Within this temperature range, methane velocities adhere to the Maxwell-Boltzmann distribution, consistent with gas-phase scaling laws ($v \propto T$), while the MSD decreases as molecular thermal motion diminishes [45]. Below 140 K, however, the MSD plateaus at near-constant values, signifying the onset of dynamic arrest. Phase-ordering kinetics dominate during methane's disorder-to-order transition, where steric confinement and lattice phonon coupling within FCC crystalline domains suppress translational mobility. This bifurcation corresponds to a phase transition from a gas-like diffusive regime to a crystalline solid state, restricting molecular motion to harmonic oscillations about equilibrium lattice positions. In the crystalline phase, translational diffusion is fully suppressed, and vibrational entropy dominates as methane molecules undergo thermally driven displacements confined by the FCC lattice potential. The observed MSD stagnation aligns with the collapse of configurational entropy during symmetry-conserved solidification, wherein interfacial

templating at NaCl-methane boundaries enforces positional order, effectively minimizing atomic-scale disorder.

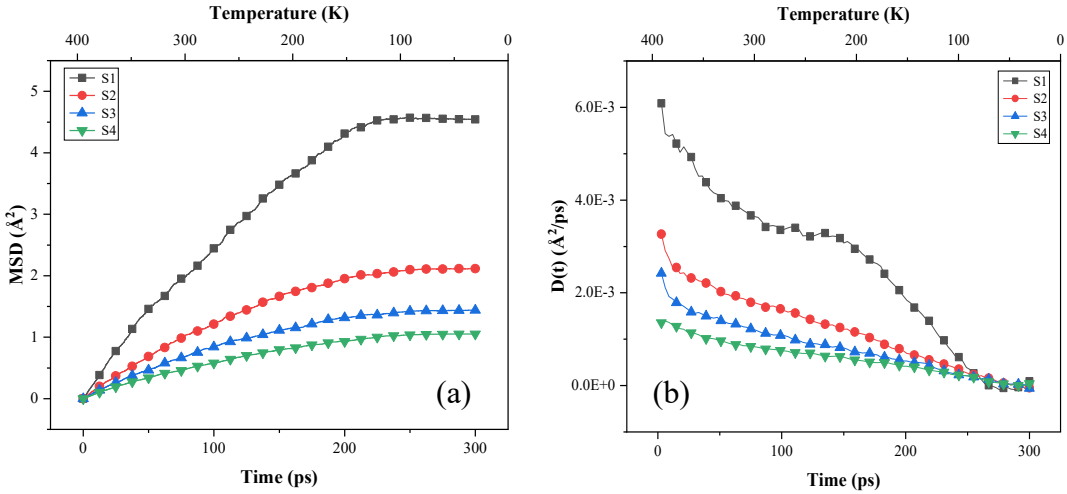


Figure 7. (a) The MSD of the Methane molecules (b) The diffusion coefficient of the methane molecules

Compared MSD, diffusion coefficient was served as a more direct indicator of gas-to-solid phase transitions due to its sensitivity to translational arrest [46]. The diffusion coefficient was calculated using Eq. (3) and presented in Figure 7(b). Its diffusivity plummeted from 0.006 Å²/ps to near-quiescent levels (0.001 Å²/ps) as the temperature approached 92 K. At this temperature, methane had almost entirely solidified. At this temperature, methane had almost entirely solidified. This sharp decline in D signifies two synergistic solidification pathways: (1) surface-mediated adsorption, where methane accumulates at nanopore interfaces via ion-dipole interactions with NaCl lattice ions, and (2) bulk-phase crystallization into FCC domains, driven by confinement-enhanced molecular packing and symmetry-conserved lattice templating. The concurrent suppression of translational mobility and emergence of vibrational entropy dominance underscore the critical role of nanoconfinement in modulating phase-transition kinetics, where interfacial and bulk mechanisms collectively govern methane's disorder-to-order transition.

Conclusions

This study employs molecular dynamics simulations to investigate methane crystallization within NaCl-constructed nanoporous channels as a novel mechanism underpinning anomalous gas storage in coalbed outburst systems. Four methane

systems under varying pressure regimes were simulated, yielding the following results:
1.Radial distribution function (RDF) analyses confirmed pronounced methane crystallization, with FCC ordering emerging prominently at 140 K. The process initiated with methane molecules forming close-packed adsorption monolayers on NaCl pore surfaces, followed by epitaxial growth into more ordered bulk FCC lattice structures—a hierarchy amplified under higher pressures (e.g., S4: 176 MPa), which elevated FCC occupancy in pore regions.
2. Near 140 K, metastable methane accumulation within nanoconfined spaces triggered localized pressure collapses approaching near-vacuum conditions, driving a complete fluid-to-solid phase transition stabilized as clathrate-like crystalline phases. This pressure collapse reflects the rapid absorption of methane from surrounding matrices into localized density anomalies (“black holes”).
3. Below critical threshold temperature (140 K), structural entropy and diffusion coefficients collapsed across all systems, marking a disorder-to-order transition from chaotic gaseous mobility to crystallized methane. Concurrently, mean squared displacement (MSD) profiles plateaued, reflecting arrested molecular motion characteristic of long-range crystalline order.
Notably, cooling-induced FCC ordering observed at 140 K underscores NaCl’s role as a crystallization template under confinement, enabled by its near-perfect lattice match with methane’s FCC phase. the findings provide mechanistic clarity on anomalous methane retention in coal matrices—bridging atomic-scale templating effects to macroscale coalbed methane (CBM) outburst risks through confinement-driven stabilization of high-density phases.

Acknowledgments
The authors gratefully acknowledge the financial support provided by the following grants: the National Natural Science Foundation of China (Grant No. 42372193).

References

[1] G. Zhang and E. Wang, "Risk identification for coal and gas outburst in underground coal mines: A critical review and future directions," *Gas Science and Engineering,* vol. 118, p. 205106, 2023.
[2] Y. Song, Q. Zou, E. Su, Y. Zhang, and Y. Sun, "Changes in the microstructure of low-rank coal after supercritical CO2 and water treatment," *Fuel,* vol. 279,

p. 118493, 2020.

[3] H. Wang, Z. Cheng, Q. Zou, Z. Li, F. Sun, H. Yang*, et al.*, "Elimination of coal and gas outburst risk of an outburst-prone coal seam using controllable liquid CO2 phase transition fracturing," *Fuel,* vol. 284, p. 119091, 2021.

[4] H. Zhang, J. Liu, and D. Elsworth, "How sorption-induced matrix deformation affects gas flow in coal seams: A new FE model," *International Journal of Rock Mechanics and Mining Sciences,* vol. 45, pp. 1226-1236, 2008.

[5] P. Guan, H. Wang, and Y. Zhang, "Mechanism of instantaneous coal outbursts," *Geology,* vol. 37, pp. 915-918, 2009.

[6] Q. Tu, Y. Cheng, S. Xue, T. Ren, and X. Cheng, "Analysis of the Coal and Gas Outburst Mechanism from the Perspective of Tectonic Movement," *Geofluids,* vol. 2021, p. 9988420, 2021.

[7] K. Jin, Y. Cheng, T. Ren, W. Zhao, Q. Tu, J. Dong*, et al.*, "Experimental investigation on the formation and transport mechanism of outburst coal-gas flow: Implications for the role of gas desorption in the development stage of outburst," *International Journal of Coal Geology,* vol. 194, pp. 45-58, 2018.

[8] F. H. An and Y. P. Cheng, "An explanation of large-scale coal and gas outbursts in underground coal mines: the effect of low-permeability zones on abnormally abundant gas," *Nat. Hazards Earth Syst. Sci.,* vol. 14, pp. 2125-2132, 2014.

[9] Y. Qin and X. Zhu, "Several Scientific Problems Faced in Developing China's Coalbed Methane Industry," *Bulletin of National Natural Science Foundation of China,* vol. 3, pp. 148-152, 2006.

[10] Z. Wang, G. Wang, C. Hao, G. Ni, W. Zhao, Y. Cheng*, et al.*, "Chemical structure and hydrocarbon generation characteristics of tectonic coal with different metamorphic degrees: Implications for gas adsorption capacity," *Gas Science and Engineering,* vol. 112, p. 204949, 2023.

[11] LI Zong-xiang, ZHANG Ming-qian, YANG Zhi-bin, DING Cong, LIU Yu, and H. Ge., "Application of FTIR and XRD in Coal Structural Analysis of Fault Tectonic[J]," *Spectroscopy and Spectral Analysis,* vol. 43, pp. 657-664, 2023.

[12] W. Sun, N. Wang, W. Chu, and C. Jiang, "The role of volatiles and coal structural variation in coal methane adsorption," *Science Bulletin,* vol. 60, pp. 532-540, 2015.

[13] A. T. Zhou, K. Wang, T. A. Kiryaeva, and V. N. Oparin, "Regularities of Two-Phase Gas Flow under Coal and Gas Outbursts in Mines," *Journal of Mining Science,* vol. 53, pp. 533-543, 2017.

[14] Z. Hao, K. Jian, S. Peng, and J. Xu, "Numerical Investigation of Coal and Gas Outbursts under Different In Situ Stresses and Gas Pressures and the Physical Characteristics of Coal," *ACS Omega,* vol. 6, pp. 13260-13274, 2021.

[15] J. W. Yan, X. B. Zhang, and Z. Zhang, "Research on geological control mechanism of coal-gas outburst," *Journal of China Coal Society,* 2013.

[16] K. P. Chen, "A new mechanistic model for prediction of instantaneous coal outbursts — Dedicated to the memory of Prof. Daniel D. Joseph," *International Journal of Coal Geology,* vol. 87, pp. 72-79, 2011.

[17] L. Si, Z. Li, Y. Yang, and R. Gao, "The stage evolution characteristics of gas transport during mine gas extraction: Its application in borehole layout for improving gas production," *Fuel,* vol. 241, pp. 164-175, 2019.

[18] S. Xue, Y. Wang, J. Xie, and G. Wang, "A coupled approach to simulate initiation of outbursts of coal and gas — Model development," *International Journal of Coal Geology,* vol. 86, pp. 222-230, 2011.

[19] C. Wang and Y. Cheng, "Role of coal deformation energy in coal and gas outburst: A review," *Fuel,* vol. 332, p. 126019, 2023.

[20] L. Li, C. Goodrich, H. Yang, K. R. Phillips, Z. Jia, H. Chen*, et al.*, "Microscopic origins of the crystallographically preferred growth in evaporation-induced colloidal crystals," *Proceedings of the National Academy of Sciences,* vol. 118, p. e2107588118, 2021.

[21] D. Y. Sun, M. Asta, and J. J. Hoyt, "Crystal-melt interfacial free energies and mobilities in fcc and bcc Fe," *Physical Review B,* vol. 69, p. 174103, 2004.

[22] B. W. van de Waal, "Cross-twinning model of fcc crystal growth," *Journal of Crystal Growth,* vol. 158, pp. 153-165, 1996.

[23] N. Di Luozzo, M. Boudard, and M. Fontana, "Transient liquid phase bonding of carbon steel components using Ni-based foils – A comprehensive joint characterization," *Materials Science and Engineering: A,* vol. 751, pp. 51-61, 2019.

[24] C. Li, M. Bescond, and M. Lannoo, "Influence of the interface-induced electron self-energy on the subthreshold characteristics of silicon gate-all-around nanowire transistors," *Applied Physics Letters,* vol. 97, 2010.

[25] M. Wu, Z. Yuan, Y. Niu, Y. Meng, G. He, and X. Jiang, "Interfacial induction and regulation for microscale crystallization process: a critical review," *Frontiers of Chemical Science and Engineering,* vol. 16, pp. 838-853, 2022.

[26] Z. Zuo, Y. Wen, and S. Zhang, "Interface-induced nucleation and growth: a new route for fabricating ordered silver nanohole arrays," *Nanoscale,* vol. 10, pp. 14039-14046, 2018.

[27] S. S. YU Hongxin, "Simulation analysis of water crystallization process," *CIESC Journal,* p. 9, 2023.

[28] Y. Li, Y. Li, C. Li, X. Zhang, F. Zeng, H. Lin*, et al.*, "Structural, mechanical, thermal and optical properties of NaCl:Ce3+ single crystals grown in large size by the Czochralski method," *Journal of Alloys and Compounds,* vol. 849, p. 156592, 2020.

[29] F. H. Cocks, "A lattice parameter method for the investigation of solid state precipitation," *Journal of Materials Science,* vol. 7, pp. 771-780, 1972.

[30] Z. R. Chong, A. H. M. Chan, P. Babu, M. Yang, and P. Linga, "Effect of NaCl on methane hydrate formation and dissociation in porous media," *Journal of Natural Gas Science and Engineering,* vol. 27, pp. 178-189, 2015.

[31] J. P. Brodholt, "Molecular dynamics simulations of aqueous NaCl solutions at high pressures and temperatures," *Chemical Geology,* vol. 151, pp. 11-19, 1998.

[32] I. Okada, Y. Namiki, H. Uchida, M. Aizawa, and K. Itatani, "MD simulation of crystal growth of NaCl from its supersaturated aqueous solution," *Journal of Molecular Liquids,* vol. 118, pp. 131-139, 2005.

[33] W. J. Zhang, B. J. Shen, Y. L. Chen, T. X. Wang, and W. Chen, "Molecular dynamics simulations about isotope fractionation of methane in shale nanopores," *Fuel,* vol. 278, 2020.

[34] K. Kadota, Y. Shirakawa, M. Wada, A. Shimosaka, and J. Hidaka, "Influence of clusters on the crystal surface of NaCl at initial growth stage investigated by molecular dynamics simulations," *Journal of Molecular Liquids,* vol. 166, pp. 31-39, Feb 2012.

[35] P. Hamal, V. Subasinghege Don, H. Nguyenhuu, J. C. Ranasinghe, J. A. Nauman, R. L. McCarley*, et al.*, "Influence of Temperature on Molecular Adsorption and Transport at Liposome Surfaces Studied by Molecular Dynamics Simulations and Second Harmonic Generation Spectroscopy," *The*

Journal of Physical Chemistry B, vol. 125, pp. 10506-10513, 2021.

[36] X. Zhang, T. Kang, B. Zhang, G. Kang, J. Kang, R. Zhang*, et al.*, "Combined Molecular Simulations and Experimental Study of Methane Adsorption on Anthracite," *Energy & Fuels,* vol. 34, pp. 12118-12125, 2020.

[37] J.-S. Yang, C.-L. Yang, M.-S. Wang, B.-D. Chen, and X.-G. Ma, "Crystallization of alkane melts induced by carbon nanotubes and graphene nanosheets: a molecular dynamics simulation study," *Physical Chemistry Chemical Physics,* vol. 13, pp. 15476-15482, 2011.

[38] S. Torquato, T. M. Truskett, and P. G. Debenedetti, "Is Random Close Packing of Spheres Well Defined?," *Physical Review Letters,* vol. 84, pp. 2064-2067, 2000.

[39] P. M. Piaggi, O. Valsson, and M. Parrinello, "Enhancing Entropy and Enthalpy Fluctuations to Drive Crystallization in Atomistic Simulations," *Physical Review Letters,* vol. 119, p. 015701, 2017.

[40] J. Liu and J. Zhang, "Nanointerface Chemistry: Lattice-Mismatch-Directed Synthesis and Application of Hybrid Nanocrystals," *Chemical Reviews,* vol. 120, pp. 2123-2170, 2020.

[41] D. Frenkel, "Order through entropy," *Nature Materials,* vol. 14, pp. 9-12, 2015.

[42] S. Yue, W. Yuan, Z. Deng, W. Xi, and Y. Shen, "In Situ TEM Observation of the Atomic Transport Process during the Coalescence of Au Nanoparticles," *Nano Lett,* vol. 22, pp. 8115-8121, Oct 26 2022.

[43] D. G. Friend, J. F. Ely, and H. Ingham, "Thermophysical Properties of Methane," *Journal of Physical and Chemical Reference Data,* vol. 18, pp. 583-638, 1989.

[44] N. Dubouis, A. Serva, R. Berthin, G. Jeanmairet, B. Porcheron, E. Salager*, et al.*, "Tuning water reduction through controlled nanoconfinement within an organic liquid matrix," *Nature Catalysis,* vol. 3, pp. 656-663, 2020.

[45] D. Camuffo, "Chapter 9 - Consequences of the Maxwell–Boltzmann Distribution," in *Microclimate for Cultural Heritage (Second Edition)*, D. Camuffo, Ed., ed Boston: Elsevier, 2014, pp. 347-366.

[46] C. C. Miller and J. Walker, "The Stokes-Einstein law for diffusion in solution," *Proceedings of the Royal Society of London. Series A, Containing Papers of a Mathematical and Physical Character,* vol. 106, pp. 724-749, 1924.